The catalytic behaviour of different sizes of dendrimer encapsulated Aun nanoparticles in the oxidative degradation of morin with H2O2.

ARTICLE *in* LANGMUIR · JULY 2015

Impact Factor: 4.46 · DOI: 10.1021/acs.langmuir.5b02020 · Source: PubMed

2 AUTHORS, INCLUDING:

Reinout Meijboom

University of Johannesburg

156 PUBLICATIONS **713** CITATIONS

Langmuir

Article

pubs.acs.org/Langmuir

Catalytic Behavior of Different Sizes of Dendrimer-Encapsulated Au_n Nanoparticles in the Oxidative Degradation of Morin with H_2O_2

Mulisa Nemanashi and Reinout Meijboom*

Department of Chemistry, University of Johannesburg, P.O. Box 524, Auckland Park 2006, Johannesburg, South Africa

Supporting Information

ABSTRACT: Different sizes of icosahedral-like dendrimer-encapsulated Au nanoparticles (Au_{55}- and Au_{147}-DENs) were prepared in the presence of generation 6 amine-terminated dendrimers (G6-PAMAM-NH_2) as a template. The synthesis is carried out by the complexation of a Au metal precursor ($AuHCl_4$) with the tertiary amine groups within the dendrimer framework. The addition of excess reducing agent, $NaBH_4$, results in the formation of Au nanoparticles encapsulated within the dendrimer cavities. The as-prepared catalysts were characterized using UV−visible (UV−vis) spectroscopy, high-resolution transmission electron microscopy (HRTEM), energy-dispersive X-ray analysis (EDX), and Fourier transform infrared (FTIR). The average sizes of Au_{55}- and Au_{147}-DENs were determined to be 1.7 ± 0.4 and 2.0 ± 0.3 nm, respectively. The catalytic activity of these Au-DEN catalysts was evaluated in the oxidative decomposition of morin by H_2O_2. Since morin has a maximum absorption band at λ 410 nm at pH 10, this catalyzed oxidation process was monitored by time-resolved UV−vis spectroscopy. The catalytic activities of these two catalysts were compared by fitting the kinetic data to the Langmuir−Hinshelwood model. This model allows the determination of adsorption constants of both morin (K_{morin}) and H_2O_2 ($K_{H_2O_2}$) on the catalyst surface. A full kinetic study for this Au-DEN-catalyzed oxidative degradation of morin is reported.

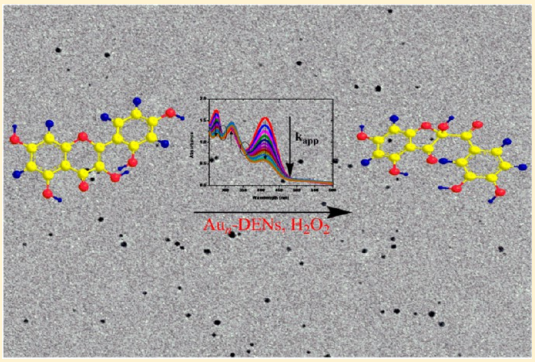

1. INTRODUCTION

Over the years, the catalytic evaluation of Au nanoparticles (Au NPs) has been given tremendous attention by scientists. Among others, Hutchings et al. has contributed significantly in this regard.[1,2] Due to their unusual optical properties, this has led to the application of Au NPs in biomedics, DNA melting, and catalysis, among others.[3−6] Haruta demonstrated for the first time in the late 1980s the use of oxide-supported nanoscale Au particles as catalysts in low-temperature CO oxidation.[7,8] Since then, supported Au NPs have been reported to exhibit catalytic activity in other gas-phase and liquid-phase reactions such as hydrocarbon hydrogenation,[9] the water−gas shift (WGS),[10] NO_x reduction by hydrocarbons,[11] and the oxidation of alkenes.[12] Traditionally, Au NPs have been considered to be catalytically active (especially for gas-phase reactions) only when they are supported on solid oxide supports. This opens a debate on whether the support plays any role in the activity of Au catalysts. Recently, Kracke et al. reported an unprecedented study on the activity of unsupported dendrimer-encapsulated Au nanoparticles (DENs) in CO oxidation.[13] The Au-DEN catalysts were kept in solution to avoid agglomeration. An increase in activity with the aging time of Au-DENs was observed, which was attributed to hydrolysis. On comparison, the activity of these catalysts was found to be comparable to that of titania-supported Au NPs. The norm has been that the dendrimer template is removed (mainly by thermal treatment) after the synthesis of Au-encapsulated nanoparticles and deposition onto solid supports but prior to catalytic evaluation.[14−16] This confirms that the effect of the support on the activity of the Au catalyst remains open for debate.[17] Therefore, it is crucial to study the catalytic behavior/performance of unsupported Au nanoparticles. The use of a dendrimer as a template during nanoparticle synthesis has a number of advantages: (i) Particles of different sizes can easily be produced by tuning the metal to dendrimer molar ratio. (ii) The dendrimer does not induce any steric effect on the accessibility of the active sites during catalytic reaction. However, in some cases, the removal of the dendrimer template by thermal processes for the immobilization of NPs on a solid support has resulted in particle agglomeration, which may subsequently hamper the activity of the catalyst.[18]

Morin is a polyphenolic dye that belongs to the group of flavonoid plant dyes. It is present in fruits, vegetables, and tea and has been used as a model substrate for studying catalytic bleaching processes in laundry detergents.[19,20] It is noteworthy to mention that, unlike many other dyes, morin is not toxic. The catalytic degradation of morin and related dyes has usually been carried out the in the presence of manganese oxide nanoparticle catalysts with H_2O_2 as the oxidant.[21,22] These manganese oxide nanoparticles are regarded to be good

Received: June 2, 2015
Revised: July 20, 2015
Published: July 21, 2015

DOI: 10.1021/acs.langmuir.5b02020
Langmuir 2015, 31, 9041−9053

catalysts for the catalytic decomposition of hydrogen peroxide.[23−25] However, more often, the synthesis of well-defined manganese oxide nanoparticles involves multistep processes and is carried out at high temperatures as compared to those (two steps) involved during DEN synthesis at room temperature.

The catalytic oxidation of dyes was observed to occur on the catalyst surface.[22,26] However, no reports are available for the use of Au nanoparticles as catalysts for the oxidation of morin. Since it has been reported that the oxidative activity of Au NPs is dependent on the size of the NPs,[27] this study aims at comparing the catalytic behavior of different sizes of Au nanoparticles using the oxidative degradation of morin as a model reaction. This is studied primarily to gain insight into the catalytic performance of Au nanoparticles prior to their use in other more complex oxidation reactions.

As mentioned previously, the use of dendrimers allows for the synthesis of well-defined NPs with different sizes, depending on the metal-to-dendrimer molar ratio. Metal NPs made up of "magic numbers" of atoms (e.g., Au_{13}, Au_{55}, etc.) result in full-shell icosahedral nanoparticles. Aiken et al.[28] reported that as the number of atoms increases, the relative active surface area decreases. Therefore, it would be interesting to investigate the catalytic behavior of different sizes of Au-DENs using the oxidation of morin as a model reaction. The Langmuir−Hinshelwood model was applied to validate the kinetic data obtained in this study. Although the preparation of dendrimer-encapsulated Au NPs has been well documented,[29−33] their use of catalysts for oxidation reactions has not been reported extensively. To the best of our knowledge, this is the first report on the use of Au nanoparticles as catalysts in the oxidative degradation of morin with H_2O_2. Moreover, a full kinetic analysis and fitting to the Langmuir−Hinshelwood model are provided. Ballauff and co-workers have employed this model to fit kinetic data for the reduction of 4-nitrophenol by $NaBH_4$ to produce 4-aminophenol.[34]

2. EXPERIMENTAL SECTION

2.1. Materials and Reagents. Generation 6 (5 wt % in methanol) dendrimer, $NaBH_4$ (99.9%), and morin hydrate (99.9%) were purchased from Sigma-Aldrich. Aqueous H_2O_2 (30% v/v) and NaOH (99.86%) were purchased from Promark Chemicals. $NaHCO_3$ (99.5%), Na_2CO_3 (99.5%), and HCl (32%) were purchased from Associated Chemical Enterprise (PTY) Ltd. All chemicals were of analytical grade and used as received. Calibration of the pH meter was done using pH 4.01 and pH 10.01 standard solutions (Scientific ADWA). All pH adjustments were performed using NaOH (0.1 M) and HCI (0.1 M). All experiments were performed using deionized water from an in-house Milli-Q system (18 ΩM·cm). The concentration of hydrogen peroxide was determined by titration.[35]

pH measurements were performed using an ORION model 520A, Schott pH electrode blueline 25. Absorption spectra for characterization and catalytic runs were obtained using a 3 mL mm quartz cuvette on a Shimadzu UV−1800 spectrophotometer. Nanoparticles were purified using a dialysis membrane (10 000 MWCO) purchased from Thermo Scientific. Particle images were obtained and analyzed using a Philips JEOL-Jem 2100 HRTEM at an acceleration voltage of 197 kV. Qualitative analysis of the particles was carried out using a GatanGIF and an Oxford INCA energy-dispersive X-ray analysis system (EDX). Samples for TEM were prepared by placing one drop of aqueous Au-DEN solution on a holey-carbon-coated Cu grid (200 mesh). Particle sizes and distributions were counted and calculated using ImageJ software.[36] FTIR analysis for the synthesis of Au_n-DENs was carried out using a Bruker Tensor 27. Samples for FTIR were prepared by mixing a few drops of a solution with KBr and drying at 70 °C. The dried samples were then ground into a fine powder and compressed into KBr pellets. All kinetic data was analyzed using Kinetic Studio software.[37] The fitting of the kinetic data was done using Origin Pro 8.5.[38] Figures were drawn using Origin Pro 8.5.[38]

2.2. Synthesis of Au_n-DENs. The synthesis of Au_n-DENs was adapted from the literature.[5,39] For the synthesis of Au_{55}-DENs, G6-PAMAM-NH_2 (0.116 g, 0.1 μmol, 5 wt % in MeOH) was added to a round-bottomed flask (10 mL), followed by removal of MeOH solvent in vacuo. After this, the dendrimer was dissolved in deionized water (10 mL) to bring the final concentration of aqueous dendrimer to 10 μM. The pH of this aqueous dendrimer solution was adjusted to approximately 2. This step is necessary to avoid the coordination of metal ions to the primary amine groups on the dendrimer as this may lead to the formation of larger particles or particle agglomeration upon reduction.[33] Aqueous Au^{3+} (55 μL, 0.1 M, 5.5 μmol) is then added to the dendrimer solution with stirring, and the mixture was allowed to stir for 30 min to allow coordination to take place. Finally, $NaBH_4$ (prepared in aqueous 0.3 M NaOH) was quickly added to this dendrimer−metal complex in 10 equiv molar excess with respect to the metal (110 μL, 0.5 M, 55 μmol). This resulted in the reduction of metal ions to form Au nanoparticles encapsulated within dendrimer cavities. The formed Au-DEN catalyst was left to stir for 1 h to allow complete reduction. Au_{147}-DENs were synthesized similarly, except that the dendrimer-to-metal molar ratio was increased to 1:147. Au-DEN catalysts were purified by dialysis against deionized water (3 × 1 L) prior to catalytic reactions. UV−vis spectra for catalyst characterization were carried out using 3 mL quartz cuvettes with deionized water as a reference for background subtraction.

2.3. Catalytic Reactions. All catalytic runs were performed in 3 mL glass or quartz cuvettes. The reactions were carried out in carbonate buffer solution made up of $NaHCO_3$ and Na_2CO_3 at pH 10. Morin exhibits a maximum absorption at λ 410 nm at this pH. The reaction is initiated by the mixing of appropriate amounts of catalyst, H_2O_2, and morin solutions in a cuvette. Unless otherwise stated, the concentrations of H_2O_2 and carbonate buffer solution were 10 and 50 mM, respectively. A stock solution of aqueous 100 mM H_2O_2 was used for H_2O_2 concentration variation studies. A 2 mM morin stock solution was prepared and was diluted into buffer to obtain a desired morin concentration in the range of 0.2 to 0.025 mM. All reactions were run at room temperature unless otherwise stated. The surface area of the nanoparticle was calculated using the average radius of the nanoparticles and the concentration of the nanoparticles, which in this case is based on the dendrimer concentration.

3. RESULTS AND DISCUSSION

Before the addition of the metal precursor to the aqueous dendrimer solution, the pH of the dendrimer solution is adjusted to acidic pH ∼2. In this acidic medium, the primary amines of the dendrimer are protonated. This avoids the coordination of metal ions with the primary amine groups on the periphery of the dendrimer which may lead to the undesired formation of dendrimer-stabilized nanoparticles (DSNs) or particle agglomeration. The desired number/concentration of Au^{3+} ions is added and coordinated with the amine groups within the dendrimer framework. After the addition of the metal salt, a drop in pH was observed (pH ∼1.9). This is because the metal salt itself is acidic. The addition of excess reducing agent ($NaBH_4$) to this dendrimer−metal complex solution results in the formation of nanoparticles encapsulated within the dendrimer framework. UV−vis spectra of the as-synthesized Au_{55}- and Au_{147}-DENs are shown in Figure 1. The aqueous dendrimer solution has an absorption band at around λ 280 nm at higher concentration. Other authors have observed this band at λ 280 nm for G4-OH, G4-NH_2, G6-OH, G2-NH_2, and G6-NH_2 PAMAM dendrimers.[40,41] This peak was assigned to the interior tertiary amine groups of the dendrimer. Contrary to the previous report

DOI: 10.1021/acs.langmuir.5b02020
Langmuir 2015, 31, 9041−9053

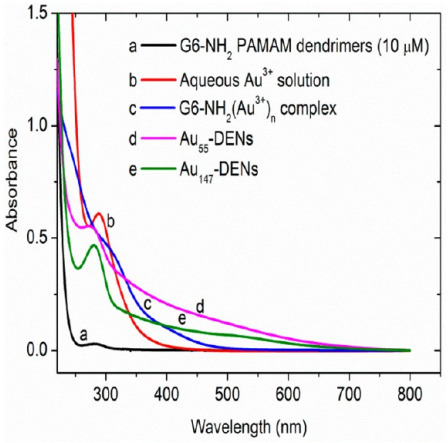

Figure 1. Aqueous UV−vis spectra of (a) Au_{55}-DENs [10 μM], (b) Au_{147}-DENs [10 μM], (c) the G6-$NH_2(Au^{3+})_n$ complex before reduction, (d) aqueous Au solution [0.55 mM], and (e) aqueous dendrimer solution (10 μM). The concentration of the DEN solution is based on the concentration of dendrimer.

by Fu and co-workers, Pande et al. reported that the intensity tends to increase with an increase in pH. Aqueous Au^{3+} solution gave an absorbance peak at around λ 290 nm. Upon the addition of $HAuCl_4$ to the aqueous dendrimer solution, a shoulder band in the range of λ 280−310 nm is observed. This shoulder band is attributed to the charge transfer between the metal and the chloride ligands, i.e., the ligand-to-metal charge transfer (LMCT). The absence of a prominent peak around λ 280 nm could be ascribed to the coordination of metal ions to the dendrimer tertiary amine groups. After the reduction of the dendrimer/metal ion complex with excess $NaBH_4$, this shoulder band disappears, indicating a complete reduction of Au^{3+} metal ions coordinated within the dendrimer cavities to form Au-DENs. The formed Au-DENs gave rise to a new absorption band at λ 280 nm. This peak around λ 280 nm is, however, more intense in the reduced DENs. This is attributed to the uncoordinated/unblocked tertiary amine groups at higher pH (pH 9.86) upon the addition of $NaBH_4$. Other authors have attributed this peak around λ 280 nm to the characteristic of a gold cluster.[42] A weak band around λ 550 nm was observed for Au_{147}-DENs. However, this band is absent for Au_{55}-DENs, indicating a population of particles with an average size of less than 2 nm. The band at λ 550 nm has been ascribed to a surface plasmon resonance (SPR) peak, confirming the presence of Au NPs with size greater than 2 nm.[30,43] Another possibility could be the overlapping of small particles that appeared as one large particle during characterization. These UV−vis spectra correlate well with the average sizes calculated on the basis of TEM results for both Au_{55}- and Au_{147}-DENs.

Fourier transform infrared (FTIR) analysis was also used to monitor the synthesis of Au_n-DEN catalysts. The spectra for aqueous generation 6 amine-terminated PAMAM dendrimer solution and a dendrimer−metal ions complex prior to and after reduction with $NaBH_4$ (i.e Au_n-DENs) were recorded and are shown in Figures S1 and S2, respectively (Supporting Information). From the information obtained, we could further confirm that there was an interaction between the dendrimer and the Au ion before and after reduction. For example, during the synthesis of Au_{147}-DENs, the absorption bands around ν 1646 and 1560 cm^{-1}, which are characteristics of the PAMAM dendrimer for the C═O stretching vibration and the C−N stretching/N−H bending, respectively, were observed.[44] Upon the addition of metal ions (Au^{3+}), these bands shift to ν 1649 and 1557 cm^{-1}. These shifts were attributed to the coordination of metal to the dendrimer. After the reduction of the dendrimer−metal complex, a further shift in absorption bands was observed. The C═O stretching vibration and C−N stretching/N−H bending shift to ν 1653 and 1558 cm^{-1}, respectively. This is ascribed to the formation of Au_n-DENs.

The as-synthesized Au-DENs were analyzed by HRTEM in order to determine the average particle diameter. Figure 2 shows representative micrographs of Au_{55}- and Au_{147}-DENs and their corresponding size distribution histograms. HRTEM images revealed that these Au nanoparticles are well dispersed and approximately spherical. The average particle sizes for Au_{55}- and Au_{147}-DENs were found to be 1.7 ± 0.4 and 2.0 ± 0.3 nm, respectively. Table 1 summarizes the calculated sizes from HRTEM analysis as well as the expected theoretical calculated sizes for both Au_{55}-DENs and Au_{147}-DENs catalysts. As can be seen in Table 1, the measured average particle sizes for both catalysts are slightly larger than the expected calculated sizes. However, for this work, we will assume that the encapsulation of nanoparticles within the dendrimer framework was successful. The particle size histograms show that both Au_n-DENs have a narrow size distribution. The presence of Au in both samples was further confirmed by EDX analysis, as can be seen in Figure 2e,f. The peaks observed for Cu are due to the Cu grids used during the TEM analysis. The presence of oxygen is from the PAMAM dendrimer while Si is from the vacuum grease used.

3.1. Catalytic Evaluation of Au_n-DENs in the Oxidative Degradation of Morin with H_2O_2. The oxidative degradation of morin was studied by monitoring the maximum absorbance of morin by time-resolved UV−vis spectroscopy. Morin hardly dissolve in water and gives only a pale yellow color. The use of buffer solution to dissolve morin solves this problem as it dissolves to give a more intense yellow color. For this reason carbonate buffer solutions were used for this study. The observed wavelength at which morin has a maximum absorbance at pH 10 was λ_{max} 410 nm. In the presence of the catalyst, the absorbance of morin with H_2O_2 at λ 410 nm decreases with time and an absorbance peak at around λ 320 nm increases (Figure 3a). The same concentration of catalyst was placed in the reference cell to suppress any UV−vis absorption associated with Au-DENs. This new absorbance has been assigned to the formed intermediate product, which is a substituted benzafuranone.[21,46] The isosbestic points observed at around λ 480, 350, and 290 nm indicate that the oxidation of morin produces only one product without any side products for the observed period. However, after a lengthy period (about after 2 h in our case), these isosbestic points start to disappear and the peak at λ 320 nm decreases. Some authors have reported shorter times for this phenomenon (t > 12 min).[21] The disappearance of these isosbestic points has been attributed to the initiation of a secondary reaction. That is, this substituted benzofuranone decomposes to 2,4-dihydroxybenzoic acid and 2,4,6-trihydroxybenzoic acid.[21,47] The rates at which these secondary products formed are not of importance to this study; therefore, our kinetic analysis was processed only within a period where morin is oxidized to give the initial product (within 1.5 h).

In the absence of a catalyst, the maximum absorption peak of morin with H_2O_2 hardly decreases even after a prolonged reaction time (Figure S3 in the Supporting Information). As a

DOI: 10.1021/acs.langmuir.5b02020
Langmuir 2015, 31, 9041−9053

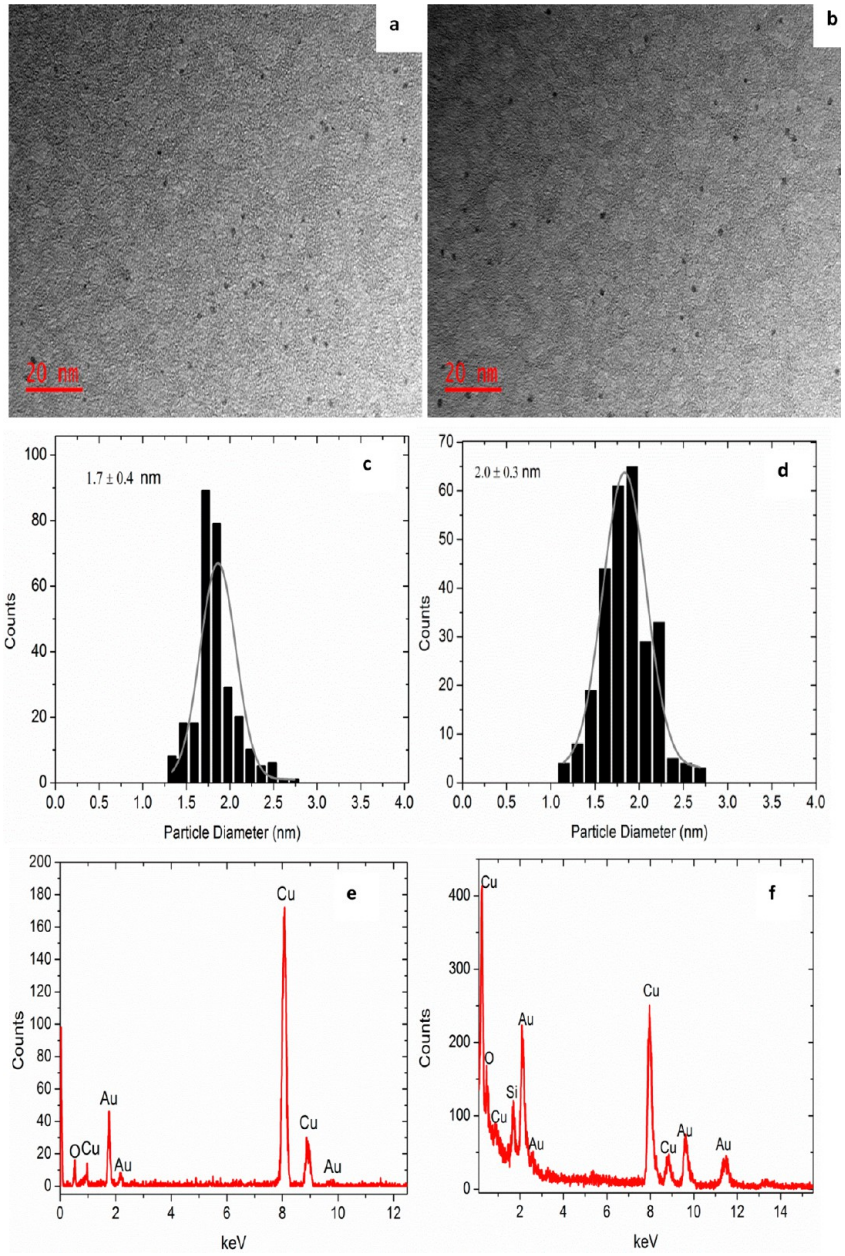

Figure 2. Representative HRTEM micrographs of (a) Au_{55}-DENs, (b) Au_{147}-DENs, and the corresponding particle size histogram of (c) Au_{55}-DENs and (d) Au_{147}-DENS, in which 260 particles were counted. (e, f) EDX spectra for Au_{55}-DENs and Au_{147}-DENs, respectively.

Table 1. Summary of Calculated and Measured Average Particle Sizes for Au_{55}-DENs and Au-$_{147}$-DENs[a]

catalyst	theoretical diameter (nm)	experimentally measured (nm)
Au_{55}-DENs	1.2	1.7
Au_{147}-DENs	1.7	2.0

[a]The theoretical sizes were calculated using equation $n = 4\pi(R - \delta)^3/3\nu_g$,[30] where n is the number of Au atoms, R is the radius of the Au nanoparticles, δ is the length of the protecting ligand (in this study, δ = 0), and ν_g is the volume of one Au atom (17 Å^3).[45]

control experiment, reactions with dendrimer and the Au^{3+}–dendrimer complex as catalysts were performed, and it was clear that they did not catalyze the oxidation of morin within the reaction time frame (Figure S4 in the Supporting Information). This observation served as initial evidence of the catalytic role played by Au-DENs in the morin oxidation reaction. Additionally, this ruled out the possibility of the formation of ultrasmall Au clusters in the reaction mixture that can potentially catalyze the reaction as reported by Corma and co-workers for the ester-assisted hydration of alkyne.[48] Therefore, the source of active species for this catalyzed oxidation of morin by H_2O_2 reported here was preformed Au nanoparticles.

The product solutions were analyzed by HRTEM to investigate if the gold nanoparticles remained dispersed during the course of the reaction. TEM images revealed that the catalyst remains fairly dispersed for both the Au_{55}-DEN- and Au_{147}-DEN-catalyzed oxidation of morin, even after the reaction (Figure S5 in the Supporting Information). This implies that there was minimal agglomeration of the nanoparticles during the reaction and suggests that this is a purely heterogeneous reaction. Additionally, this serves as evidence

DOI: 10.1021/acs.langmuir.5b02020
Langmuir 2015, 31, 9041−9053

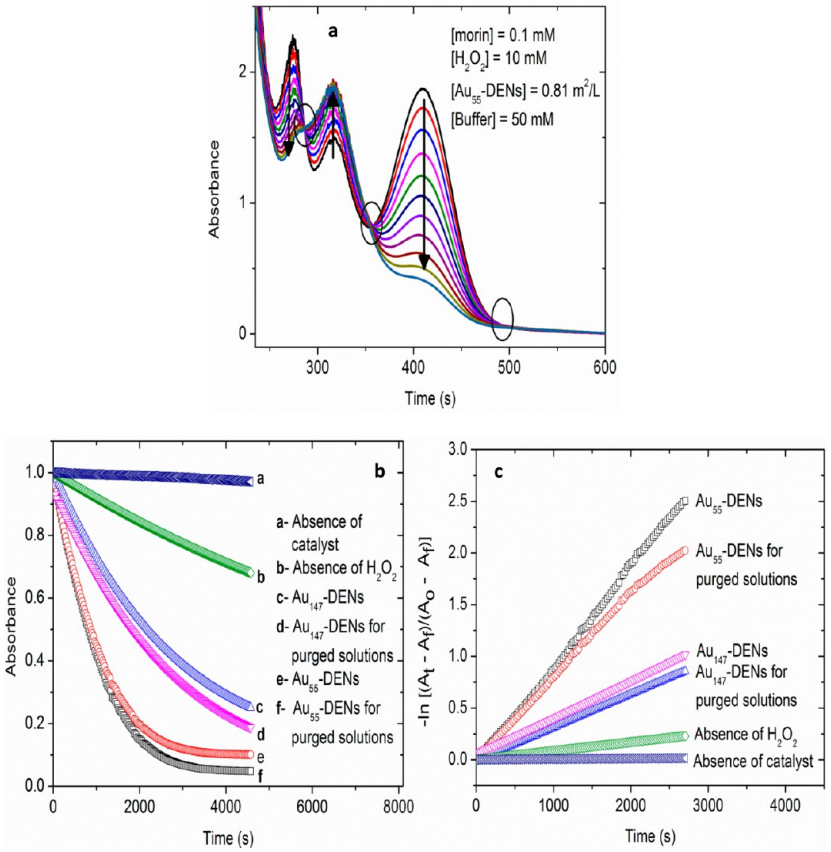

Figure 3. Time-revolved UV−vis spectra of morin solution (0.1 mM) with H_2O_2 (10 mM) in a carbonate buffer solution (50 mM) at pH 10 and 298 K. (a) Catalytic oxidation of morin in the presence of Au-DEN catalysts (spectra taken every 10 min). (b) Kinetic spectral changes and (c) the corresponding first-order plots for the catalytic oxidation of morin as a function of time with and without catalyst. [Morin], 0.1 mM; [H_2O_2], 10 mM; [Au_{55}-DENs], 0.81 m^2/L; [carbonate buffer], 50 mM, pH 10, T = 298 K.

that the nanoparticles remain intact during the reaction and that there was no leaching of atoms into the solution as observed in other nanoparticle-catalyzed reactions.[49] However, it is noteworthy to mention that it is difficult to separate the catalyst from the reaction products for reuse under the reaction conditions used for this current study.

Since the decrease in the absorption of morin at λ 410 nm is directly proportional to the morin concentration, the data obtained here can be used to determine the kinetics of the catalyzed oxidation reaction. The concentration of morin was observed to decrease nonlinearly with time when excess hydrogen peroxide was used (100-fold molar excess) in the presence of the Au_n-DEN catalyst (Figure 3b). A linear relation was obtained when the logarithmic of the data was plotted against time, confirming that this reaction follows pseudo-first-order kinetics with respect to morin concentration (Figure 3c). In order to investigate the influence of oxygen from air, experiments in the absence of H_2O_2 were performed. The oxidation of morin was observed to occur slowly (k_{obs} = 1.1 × 10^{-6} s^{-1}) in the absence of H_2O_2. More importantly, in the presence of H_2O_2 the apparent rate constant observed for purged solutions was not significantly different from what had been observed in the presence of air (Figure 3). These results suggest that the role of oxygen in the presence of H_2O_2 is negligible. These observations are similar to what has been reported by Polzer et al. for the manganese oxide-catalyzed oxidation of morin by H_2O_2.[21] Normally, during a catalytic reaction, time is required for NP restructuring during the catalytic reaction, and thus an induction period is often observed.[4,50] However, in our case, the reaction was observed to commence as soon as the required amount of H_2O_2 was added to the reaction solution.

The rate at which this oxidation reaction is occurring as a function of catalyst amount/concentration was studied. The apparent rate constant, k_{app}, is proportional to the concentration of the catalyst in the system. As can be seen in Figure 4, a linear increase in k_{app} with increasing catalyst amount was observed. This is attributed to an increased surface area available to participate in the catalytic reaction. However, this increase in the apparent rate constant is observed only for a certain maximum catalyst concentration for fixed reaction conditions. Therefore, it is important to determine the right amount of catalyst for a kinetic study. This observation confirms that the reaction kinetics measured in this study are not diffusion-controlled. The effect of buffer concentration on the rate of reaction was also studied. There was no significant increase in the rate constant with increasing carbonate concentration (Figure S6). This suggests that the role of carbonate is mainly for the formation of peroxycarbonate ion radicals, which help to initiate the reaction in the presence of H_2O_2 and catalyst. As a result, the influence of buffer concentration was not considered during kinetic analysis. However, some authors have reported a second-order increase in the rate constant as the hydrogen carbonate buffer increases.[51]

DOI: 10.1021/acs.langmuir.5b02020
Langmuir 2015, 31, 9041−9053

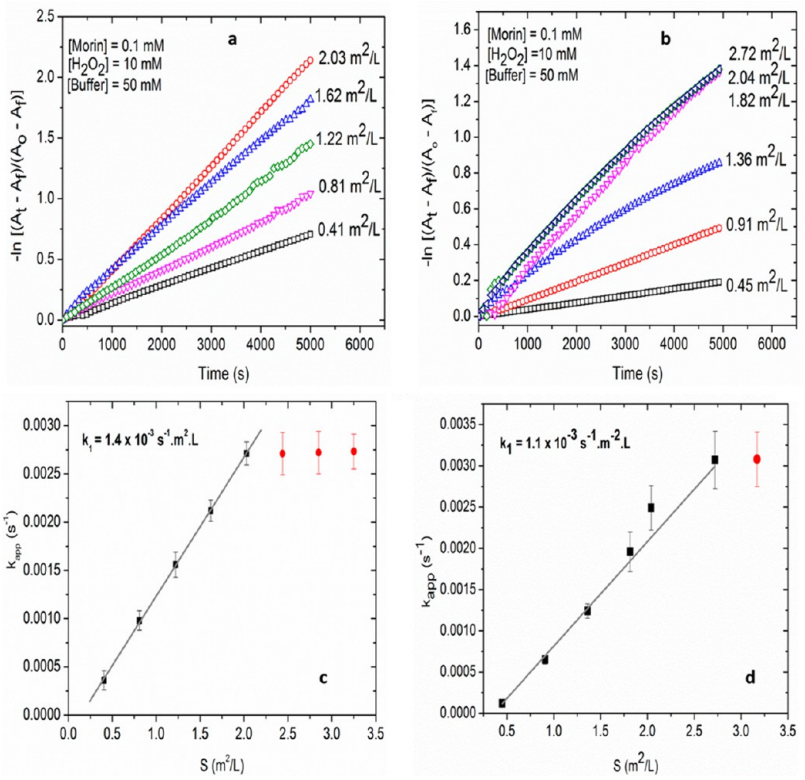

Figure 4. Influence of catalyst concentration (volume-normalized surface area) on the apparent rate constant in the catalyzed oxidation of morin and the corresponding first-order plot for each catalytic run for Au_{55}-DENs (a, c) and Au_{147}-DENs (b, d). [Morin] = 0.1 mM, [H_2O_2] = 10 mM, [buffer] = 50 mM, pH 10, T = 298 K.

Table 2. Parameter Calculated to Disqualify the Possibility of Diffusion Limitations for Au_{55}- and Au_{147}-DEN-Catalyzed Oxidation of Morin by H_2O_2[a]

catalyst	k_{app} ($\times 10^{-4}$ s^{-1})[b]	δ ($\times 10^{-9}$ m)	β ($m \cdot s^{-1}$)	a (m^{-1})	$DaII$ ($\times 10^{-5}$)	k_{bm} ($\times 10^{6}$ $s^{-1} \cdot m^{-2} \cdot L$)
Au_{55}-DENs	9.8	6.7	0.081	810	1.49	3.5
Au_{147}-DENs	6.5	6.7	0.081	910	0.88	4.1

[a]The calculated $DaII$ value and k_{bm} values suggested that the reaction kinetics measured were not diffusion-controlled for both systems. [b]k_{app} at [morin] = 0.1 mM, [H_2O_2] = 10 mM, [Au_{55}-DENs] = 0.81m^2/L, [Au_{147}-DENs] = 0.91 m^2/L, and T = 298 K.

For a known k_{app}, the volume-normalized surface of the catalyst, S, can easily be calculated using eq 1

$$k_1 = \frac{k_{app}}{S} \tag{1}$$

where k_{app} is the apparent rate constant and k_1 is the surface-normalized rate constant given by the slope of the linear plot (Figure 4c,d).

In order to exclude the possibility of diffusion control in this study, some parameters were calculated. The reaction is considered to be diffusion-controlled if the reaction turnover at the surface is faster than the diffusion of the reactants, with the assumption that the reaction is occurring at the surface of the nanoparticle catalyst. These phenomena can be determined by calculating the second Damköhler number ($DaII$), shown in eq 2

$$DaII = \frac{k_{app}[\text{morin}]^{n-1}}{\beta a} \tag{2}$$

where k_{app} is the apparent rate constant, [morin] is the concentration of the reactant, β is the mass transport coefficient, a is the area of the interface, which in this study is the volume-normalized area of the Au nanoparticles, and n is the order of the reaction (first order for this study). The parameter β can be further defined as the diffusion coefficient divided by the characteristic length scale δ over which mass transport takes place. The calculated diffusion constant of morin was previously reported to be 5.45 $\times$ 10^{-10} m^2/s.[52] A number of authors have also used the same method to disqualify the possibility of diffusion control taking place in their kinetic studies.[4,39,53] The value of $DaII$ was determined to be considerably smaller than 1 for both catalytic systems. In order to completely exclude the possibility of diffusion control in the kinetic measurements obtained here, a derivation of Fick's second law can be applied. The derivative of Fick's second law is given in eq 3, where k_{bm} is the bimolecular rate constant, r is the average radius of the nanoparticle, and r/D and $1/k_{et}$ are diffusion and electronic terms, respectively. For a diffusion-controlled reaction, this diffusion term must be far greater than the electronic term, i.e., $r/D \gg 1/k_{et}$. Therefore, eq 3 can be expressed in terms of the Scholuchowski equation (eq 4).

$$\frac{1}{k_{bm}} = \frac{1}{4\pi r^2}\left(\frac{1}{k_{et}} + \frac{r}{D}\right) \tag{3}$$

DOI: 10.1021/acs.langmuir.5b02020
Langmuir 2015, 31, 9041−9053

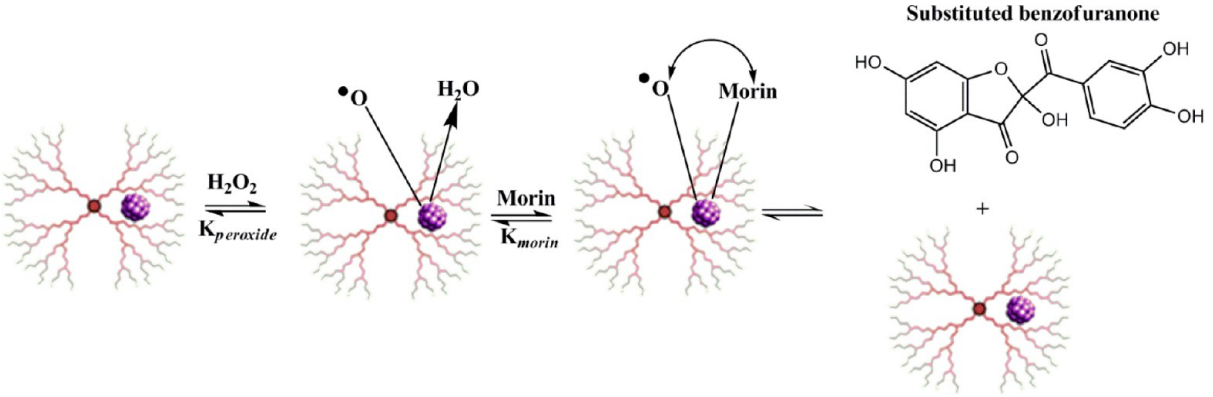

Figure 5. Illustration of the adsorption of species on the metal nanoparticle surface during the oxidation of morin according to the Langmuir–Hinshelwood mechanism. Both reactants must be adsorbed on the catalyst surface before the reaction can commence. H_2O_2 forms oxygen radicals on the surface of the catalyst followed by the adsorption of morin onto the nanoparticle surface, which undergoes reaction on the surface with the active oxygen radicals (rate-determining step).

$$k_{bm} = 4\pi rD \tag{4}$$

The experimentally obtained values for the normalized rate constant, k_1, were determined to be 1.4×10^{-3} and 1.1×10^{-3} $s^{-1}\cdot m^{-2}\cdot L$ for Au_{55}-DENs and Au_{147}-DENs, respectively (Figure 4c,d). These values are far less than the calculated bimolecular rate constants of 4.1×10^6 and 3.5×10^6 $s^{-1}\cdot m^{-2}\cdot L$ for Au_{55}-DEN and Au_{147}-DEN catalysts, respectively (Table 2), thus ruling out mass transport problems. These bimolecular rate constant values are determined by using eq 4 and further multiplying them by Avogadro's number. Both calculated *DaII* parameters for Au_{55}-DENs and Au_{147}-DENs are given in Table 2. On the basis of these values we can exclude mass transport limitations under the kinetic conditions reported here.

3.1.1. Treatment of Kinetic Data According to the Langmuir–Hinshelwood Model. Given the aforementioned findings, we modeled the data for Au-catalyzed morin oxidation with H_2O_2 in terms of the Langmuir–Hinshelwood mechanism. This model describes that both reactants must first be adsorbed onto the surface of the catalyst in order for the reaction to commence. We and others have studied the reduction of nitrophenol using a similar approach.[4,5,53] Figure 5 illustrates a schematic representation of this mechanism.

As shown in Figure 5, H_2O_2 adsorbs on the catalyst surface, resulting in adsorbed active oxygen species and the release of water molecules. The rate-determining step occurs as morin molecules also absorb on the catalyst surface and react with active oxygen species. Both of these processes for the adsorption of morin and hydrogen peroxide are assumed to be fast and reversible.[54] The decomposition product is released from the catalyst surface, allowing the resulting free active site to be available for another catalytic reactant. The desorption of the product is assumed to be fast and irreversible and is not considered in the kinetic analysis.

The rate for the oxidation of morin can be expressed by the rate law shown in eq 5.

$$-\frac{d[morin]}{dt} = k[morin]^n[H_2O_2]^m[catal]^l \tag{5}$$

The catalyst surface area remains constant, as evidenced by TEM images (Figure S1 in the Supporting Information). Thus, the rate law can include the catalyst surface area, S, for a catalytic reaction as a constant. Since H_2O_2 is present in large excess with respect to the morin concentration, it is assumed to remain approximately constant throughout the reaction. As explained previously, this reaction is observed to follow pseudo-first-order kinetics (Figure 3c); therefore, this rate law can be expressed as eq 6

$$-\frac{d[morin]}{dt} = k_1 S[morin]^n = k_{app}[morin] \tag{6}$$

where [morin] is the concentration of morin at a given time t, S is the volume-normalized surface area, and k_1 is the surface-normalized apparent rate constant. It should be noted that, for this study, the concentration of the catalyst was based on the dendrimer concentration used for the preparation of a particular Au_n-DEN catalyst. From that concentration and the total value of the reaction system, the volume-normalized surface area of the catalysts were calculated. From the Langmuir–Hinshelwood mechanism, which assumes the adsorption of both reacting species on the surface of the catalyst, the rate equation can be written as eq 7

$$-\frac{d[morin]}{dt} = kS\theta_{morin}\theta_{H_2O_2} \tag{7}$$

where θ_{morin} and $\theta_{H_2O_2}$ are the surface coverages of morin and hydrogen peroxide, respectively, and k is the actual rate constant on the surface. These surface coverages for morin and H_2O_2 can be expressed by Freundlich isotherms given in eqs 8 and 9

$$\theta_{morin} = \frac{(K_{morin}[morin])^n}{1 + (K_{morin}[morin])^n + (K_{H_2O_2}[H_2O_2])^m} \tag{8}$$

$$\theta_{H_2O_2} = \frac{(K_{H_2O_2}[H_2O_2])^m}{1 + (K_{morin}[morin])^n + (K_{H_2O_2}[H_2O_2])^m} \tag{9}$$

where K_{morin} and $K_{H_2O_2}$ are the adsorption constants for morin and H_2O_2, respectively, for both equations; m and n are Freundlich constants (not orders), and the latter can be used to describe the heterogeneity of the surface of the nanoparticle catalyst.[55] The substitution of eqs 8 and 9 into eq 7 results in eq 10, which relates all of the parameters involved in the Langmuir–Hinshelwood model.

DOI: 10.1021/acs.langmuir.5b02020
Langmuir 2015, 31, 9041–9053

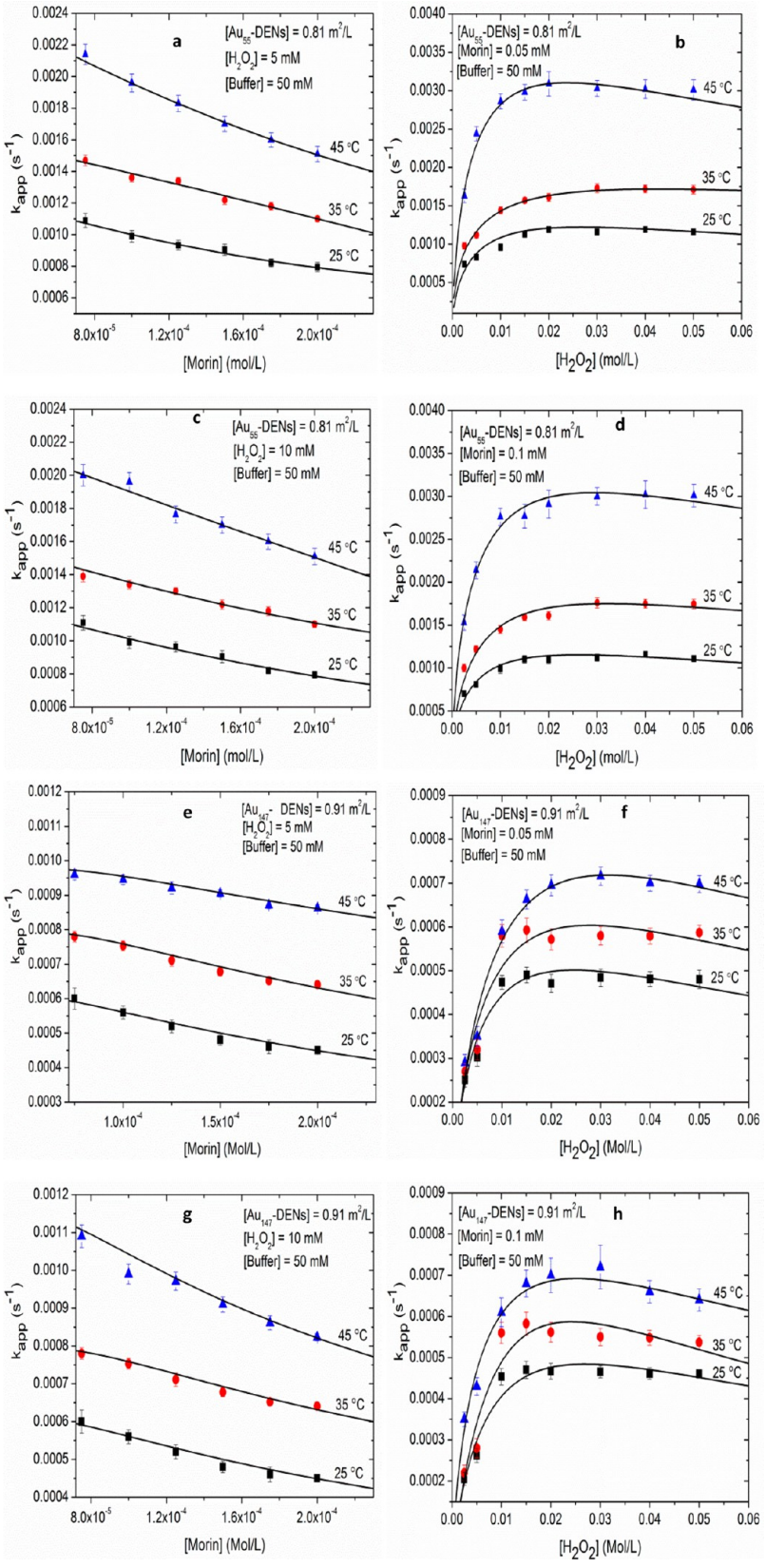

Figure 6. Analysis of kinetic data in terms of the Langmuir−Hinshelwood model at three different temperatures (25, 35, and 45 °C). (a, c, e, g) Influence of morin concentration for Au_{55}-DENs (a, c) and Au_{147}-DENs (e, g) on k_{app} at constant peroxide concentration (5 mM H_2O_2 for a and e; 10 mM H_2O_2 for c and g, respectively). (b, d, f, h) Dependencies of k_{app} on the concentration of H_2O_2 for Au_{55}-DENs (b, d) and Au_{147}-DENs (f, h) at a constant concentration of morin (0.05 mM morin for b and f; 0.1 mM morin for d and h). The pH and concentration of carbonate buffer remained constant (pH 10 and 50 mM) throughout all experiments. The normalized surface areas used for this kinetic study for Au_{55}-DENs and Au_{147}-DENs were 0.81 and 0.91 m^2/L, respectively.

DOI: 10.1021/acs.langmuir.5b02020
Langmuir 2015, 31, 9041−9053

Table 3. Summary of the Surface Rate Constant and Adsorption Constants of Morin and H_2O_2 for the Au_{55}-DENs and Au_{147}-DEN-Catalyzed Oxidation of Morin by H_2O_2 Obtained from the Best Fit According to the Langmuir–Hinshelwood Model

catalyst	temp (°C)	k [mol·(m^2·s)$^{-1}$] (× 10^{-6})	K_{morin} [L·mol^{-1}]	$K_{H_2O_2}$ [L·mol^{-1}]	n	m
Au_{55}-DENs[a]	25	5.6 ± 1.6	686 ± 49	41 ± 2	1 ± 0.02	0.9 ± 0.03
	35	4.9 ± 1.4	554 ± 69	27 ± 3	1 ± 0.03	0.6 ± 0.02
	45	6.9 ± 1.9	886 ± 43	46 ± 5	1 ± 0.03	0.8 ± 0.01
Au_{147}-DENs[a]	25	5.9 ± 1.7	763 ± 69	30 ± 2	1 ± 0.04	0.8 ± 0.04
	35	8.7 ± 1.3	1092 ± 76	51 ± 1	1 ± 0.04	0.9 ± 0.02
	45	7.0 ± 2.1	927 ± 72	36 ± 0.9	1 ± 0.03	0.7 ± 0.04
catalyst	temp (°C)	kS (mol·m^2·L^{-2}·s^{-1}) (× 10^{-6})	K_{morin} [L·mol^{-1}]	$K_{H_2O_2}$ [L·mol^{-1}]	n	m
Comparison with the Literature						
MnOx@SPB[b]	15	1.36 ± 0.26	3866 ± 1157	245 ± 20	1 ± 0.04	0.9 ± 0.03
	20	1.86 ± 0.41	3434 ± 1174	255 ± 24	1 ± 0.04	0.9 ± 0.02
	25	2.48 ± 0.82	3145 ± 1623	175 ± 18	1 ± 0.07	0.9 ± 0.04
	30[c]	3.48 ± 1.34	2631 ± 1529	165 ± 17	1 ± 0.07	0.9 ± 0.04

[a]This work. [b]MnO_xNP@SPB-catalyzed oxidation of morin.[21]

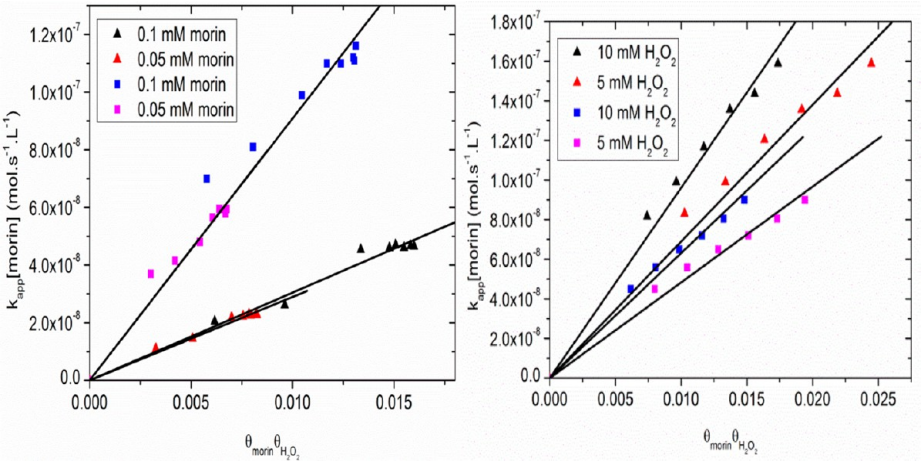

Figure 7. Kinetic plots for the reduction of morin according to the Langmuir–Hinshelwood model at constant morin and H_2O_2 concentrations. The plots are products of the apparent rate constant, k_{app}, and the concentration of morin, [morin], against the product of surface coverage, $\theta_{morin}\theta_{H_2O_2}$. The normalized surface areas used for this kinetic study for Au_{55}-DENs and Au_{147}-DENs were 0.81 and 0.91 m^2/L, respectively. The squares are for Au_{147}-DENs, and the triangles are for Au_{55}-DENs.

$$k_{app} = \frac{kSK^{n}_{morin}[morin]^{n-1}(K_{H_2O_2}[H_2O_2])^{m}}{(1 + (K_{morin}[morin])^{n} + (K_{H_2O_2}[H_2O_2])^{m})^{2}} \quad (10)$$

It is now clear that, for a known experimentally obtained apparent rate constant, k_{app}, the surface rate constant, k, and adsorption constants for both morin and H_2O_2 can be determined. The effect of morin (at constant [H_2O_2]) and H_2O_2 (at constant [morin]) concentrations on the apparent rate constant was also studied, and the results for the best fit according to the Langmuir–Hinshelwood model are shown in Figure 6. Solid lines in Figure 6 are the best fit for eq 10. As can be seen, for all three different temperatures, the apparent rate constant was found to be nonlinearly decreasing as the morin concentration increases. This can be attributed to the fact that as the concentration increases, the NP catalyst surface is mainly covered by morin. This also makes it difficult for the peroxide to be adsorbed onto the active sites of the catalyst, and this consequently slows the reaction rate. Similarly, the rate constant increases as the peroxide concentration increases. However, as soon as all active sites of the catalysts are covered or blocked, the rate does not appear to increase further. This trend was also observed for the oxidation of morin on MnO_x nanoparticles[21] and the reduction of nitrophenol.[4,39,54]

The surface rate constants, k, K_{morin}, and $K_{H_2O_2}$, were all found to be temperature-dependent. All of these parameters were observed to increase with increasing temperature for both catalysts studied (Au_{55}- and Au_{147}-DENs). The increase in $K_{H_2O_2}$ was small as compared to the increase in K_{morin} for a given set of temperatures for both catalysts. Both the apparent rate constant and the surface rate constant were found to increase with decreased nanoparticle size and temperature, i.e., higher for Au_{55}-DENs than for Au_{147}-DENs. Although a slightly higher volume-normalized surface area was used for Au_{147}-DENs than for Au_{55}-DENs for the kinetics used for L-H data fitting, Au_{55}-DENs generally gave a higher rate constant under similar reaction conditions. This observation clearly shows the dependence of the rate constant on the size of the Au nanoparticles. On the assumption that the synthesis of particles with a well-defined shape and full-shell magic numbers (Au_{55} and Au_{147}) was successful, it would be meaningful to suggests that Au_{55}-DEN has the lowest coordination number (CN) compared to Au_{147}-DEN at the corner and edge atoms (on which reactants get absorbed) that are responsible for the

DOI: 10.1021/acs.langmuir.5b02020
Langmuir 2015, 31, 9041–9053

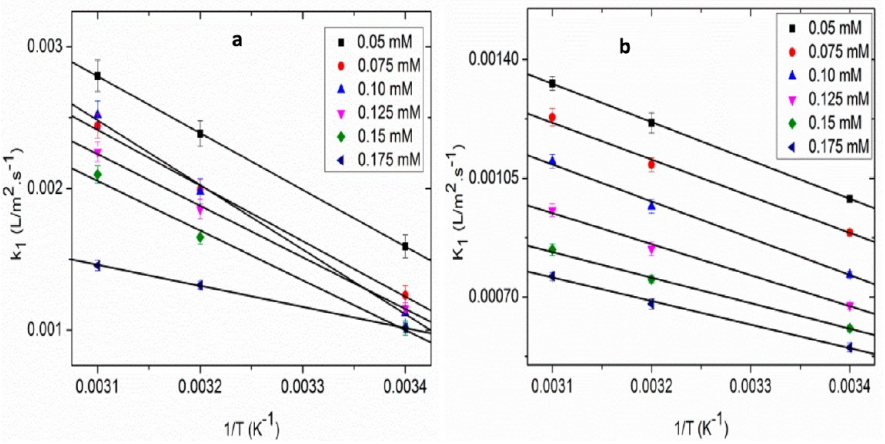

Figure 8. Arrhenius plots for the surface-normalized rate constant, k_1, for different concentration of morin at 10 mM H_2O_2, taken from data used for Langmuir–Hinshelwood fitting in Figure 6 at three different temperatures. (a) Au_{55}-DENs and (b) Au_{147}-DENs.

activity of Au catalysts. This coordination number has been reported to decrease with an increased number of corner and edge atoms.[27] As a result, Au_{55}-DENs showed higher activity than Au_{147}-DENs for this study. However, the apparent rate constant, k_{app}, was found to be significantly higher than the surface rate constant, k. This is presumably because the adsorption equilibrium on the catalyst surface for both reactants is fast; therefore, the surface rate becomes smaller than the apparent rate constant. Other authors have observed an increase in catalytic activity for a decreased nanoparticle size for the reduction of 4-nitrophenol.[53,56] Although normalized surface areas were used for this study, these results suggest that the activity of the catalyst for NPs of different sizes does not solely depend on the catalyst surface area. Therefore, the same surface area does not always give the same kinetic results for NPs of different sizes. The results for all parameters obtained from the Langmuir–Hinshelwood model are summarized in Table 3.

In order to determine the reliability of the obtained kinetic data, the surface coverage values of both morin and H_2O_2 (θ_{morin} and $\theta_{H_2O_2}$) were calculated using eqs 8 and 9, respectively, for both catalysts. The product of $\theta_{morin}\theta_{H_2O_2}$ was plotted against k_{app}[morin]. The slope of these linear lines, illustrated in Figure 7, should compare well with the products of the kinetic constant, k, and the surface area of the nanoparticles, S, according to eqs 11a and 11b. Equation 11a is derived by substituting eqs 8 and 9 into eq 10 and can be further simplified to give eq 11b.

$$k_{app}[\text{morin}] = kS\theta_{morin}\theta_{H_2O_2} \tag{11a}$$

$$kS = \frac{k_{app}[\text{morin}]}{\theta_{morin}\theta_{H_2O_2}} \tag{11b}$$

The plot for data obtained by varying the concentrations of both morin and H_2O_2 is shown in Figure 7. Considering the error involved in calculating the values of θ_{morin} and $\theta_{H_2O_2}$, the slopes of these lines were found to compare well with the calculated values for the product of the kinetic constant, k, and the surface area of the nanoparticles, S. On the basis of these fittings we can conclude that the Langmuir–Hinshelwood was an appropriate model for the comparison of the two catalysts, Au_{55}-DENs and Au_{147}-DENs.

3.1.2. Dependence of Parameters on the Temperature. As can be seen in Figure 8, the surface-normalized rate constant, k_1, was found to decrease at a given temperature for various morin concentrations and constant H_2O_2 concentration for both catalysts studied. This Arrhenius plot signifies the observed increase in the adsorption constant of morin as the temperature increases for both catalysts. This trend is more prominent when the adsorption constants for both K_{morin} and $K_{H_2O_2}$ are plotted against the inverse temperature (Figures S7 and S8 in the Supporting Information). Although it is tempting to assume the same for H_2O_2, the adsorption of H_2O_2 on the catalyst surface is a complex process and cannot be explained with certainty.[25] Similar observations have been reported for the adsorption of $NaBH_4$ on the catalyst surface in hydrolysis reactions.[57]

The change in the enthalpy of activation, $\Delta H^{\ddagger}$, and the change in entropy, $\Delta S^{\ddagger}$, for k_{app}, k, K_{morin}, and $K_{H_2O_2}$ were calculated using the van't Hoff equation shown in eq 12. The Eyring plots from which both of these parameters were calculated are shown in Figures S12–S16 (Supporting Information)

$$\ln k = \frac{\Delta H^{\ddagger}}{RT} + \frac{\Delta S^{\ddagger}}{R} \tag{12}$$

where $\Delta H^{\ddagger}$ is the change in enthalpy, $\Delta S^{\ddagger}$ is the change in entropy, R is the universal gas constant, and T is the temperature in Kelvin. By using the values obtained in eq 12, the Gibbs free energy of activation, $\Delta G^{\ddagger}$, can be calculated for each variable using eq 13.

$$\Delta G^{\ddagger} = \Delta H^{\ddagger} - T\Delta S^{\ddagger} \tag{13}$$

The enthalpy of activation, $\Delta H^{\ddagger}$, was determined to be positive for all systems studied, indicating that the catalyzed oxidation of morin was an endothermic process. From the values of the Gibbs free energy, the reaction appeared to be nonspontaneous. The activation energies for k_{app} and the surface rate, k, can be calculated using the Arrhenius equation given by eq 14. where E_a is the activation energy, k is the rate constant (on the surface), R is the universal gas constant, A is referred to as a frequency factor, and T is the temperature in Kelvin.

$$\ln k = -\frac{E_a}{RT} + \ln A \tag{14}$$

DOI: 10.1021/acs.langmuir.5b02020
Langmuir 2015, 31, 9041–9053

Table 4. Summary of All Thermodynamic Parameters Calculated for the Catalyzed Oxidation of Morin by H_2O_2 for Both Au_{55}-DENs and Au_{147}-DENs

catalyst	parameter	$\Delta H^{\ddagger}$ (kJ·mol^{-1})	$\Delta S^{\ddagger}$ (J·mol^{-1}·K^{-1})	$\Delta G^{\ddagger}$ (kJ·mol^{-1})	E_a (kJ·mol^{-1})	ref
Au_{55}-DENs	k_{app}	21 ± 2	−234 ± 6	91 ± 1.2	16.6 ± 1.3	TW
	k	15 ± 1	−295 ± 5	103 ± 1.9	9.8 ± 0.9	TW
	k_1	28 ± 3	−209 ± 6	90 ± 1.0	13.6 ± 1.4	TW
	K_{morin}	16 ± 2	−138 ± 3	57 ± 0.7		TW
	$K_{H_2O_2}$	6 ± 0.6	−194 ± 4	64 ± 0.8		TW
Au_{147}-DENs	k_{app}	20 ± 2	−239 ± 7	91 ± 0.9	17.6 ± 1.9	TW
	k	12 ± 0.9	−308 ± 9	104 ± 2.0	12.1 ± 0.7	TW
	k_1	16 ± 1	−253 ± 6	91 ± 2.1	19.4 ± 1.1	TW
	K_{morin}	17 ± 0.8	−134 ± 3	57 ± 1.0		TW
	$K_{H_2O_2}$	9 ± 0.5	−295 ± 4	97 ± 1.9		TW
MnO_xNP@SPB[a]	kS				45.8 ± 7.0	21
	K_{morin}	−20 ± 8.7	30 ± 0.2	−28.940		21
	$K_{H_2O_2}$	−21 ± 3.1	−26 ± 11	−13.252		21
(PANI)/MnO_2[b]	k_{app}	32	−156	80	35	58

[a]Oxidation of morin. [b]Oxidation of indigo carmine.

The Arrhenius plots and their corresponding equations used for the calculation of activation energies for k_{app}, surface rate, k, and normalized rate constant, k_1, are shown in Figures S9−S11 (Supporting Information). The activation energy for k_{app} depends on the adsorption constants for both morin and H_2O_2. Therefore, it would be ideal to carry out some further experiments to account for this; however, the information obtained for this study is enough to serve as a foundation for future investigations.

Ballauff and co-workers have recently published some of these thermodynamic parameters on the catalyzed oxidation of morin by H_2O_2, albeit using a different catalyst, Mn_xO_2.[21] Therefore, the thermodynamic values reported in this study can be used in the future for the investigation of the catalytic behavior of Au-DENs during the reaction. The activation energy for the Au_{55}-DENs catalyst was calculated to be smaller than that of Au_{147}-DENs. This was expected, as there seems to be a correlation between increased activity with a decrease in nanoparticle size.[27] Similar observations were reported by our group, although for a different reaction.[53] The activation energy for the surface rate, k, was found to be smaller as compared to the calculated E_a of k_{app} for both catalytic systems. Table 4 summarizes the thermodynamic parameters calculated for the oxidation of morin by H_2O_2. The few reports available on the thermodynamic parameter values for morin oxidation and other organic dyes have also been included in Table 4 for comparison.

4. CONCLUSIONS

Dendrimers have been used as templates for the formation of Au NPs encapsulated within the cavities of the dendrimer framework. Different sizes of Au NPs can be prepared with the use of dendrimers as a template by varying the metal-to-dendrimer molar ratio. The dendrimer template does not passivate the substrate from accessing the active metal site. Au-DENs can be used as catalysts for the catalyzed oxidation of morin by H_2O_2. The rate constant was observed to decrease with an increased particle size, and hence Au_{55}-DEN was more active than the Au_{147}-DEN for the oxidative degradation of morin. The nanoparticles do not agglomerate during the reaction, even at higher temperature (35 °C for this study). The Langmuir−Hinshelwood mechanism was successfully used to study the catalytic behavior and surface reactivity of the nanoparticles. On the basis of the calculated value for enthalpy change (positive) for all systems studied, the catalyzed oxidation of morin is an endothermic reaction.

■ ASSOCIATED CONTENT

Supporting Information

The Supporting Information is available free of charge on the ACS Publications website at DOI: 10.1021/acs.langmuir.5b02020.

FTIR and UV−vis spectra. HRTEM images. Rate constant vs carbonate buffer concentration. Absorption constant of morin vs temperature. Arrhenius and Eyring plots. (PDF)

■ AUTHOR INFORMATION

Corresponding Author

*Tel: +27(0)11 5592367. Fax: +27(0)11 5592816. E-mail: rmeijboom@uj.ac.za.

Notes

The authors declare no competing financial interest.

■ ACKNOWLEDGMENTS

The University of Johannesburg and NRF (grant specific unique reference (UID) 85386) and Sasol R&D are greatly appreciated for their financial support. We also acknowledge Mr. D. Harris and Dr. R. Meyer (Shimadzu S.A.) and CSIR for the equipment used for this study.

■ REFERENCES

(1) Hutchings, G. J. Catalysis: A Golden Future. *Gold Bull.* **1996**, *29*, 123−130.

(2) Hashmi, A. S. K.; Hutchings, G. J. Gold Catalysis. *Angew. Chem., Int. Ed.* **2006**, *45*, 7896−7936.

(3) Sardar, R.; Funston, A. M.; Mulvaney, P.; Murray, R. W. Gold Nanoparticles: Past, Present, and Future. *Langmuir* **2009**, *24*, 13840−13851.

(4) Wunder, S.; Lu, Y.; Albrecht, M.; Ballauf, M. Catalytic Activity of Faceted Gold Nanoparticles Studied by a Model Reaction: Evidence for Substrate-Induced Surface Restructuring. *ACS Catal.* **2011**, *1*, 908−916.

DOI: 10.1021/acs.langmuir.5b02020
Langmuir 2015, 31, 9041−9053

(5) Nemanashi, M.; Meijboom, R. Synthesis and Characterization of Cu, Ag and Au Dendrimer-Encapsulated Nanoparticles and their Application in the Reduction of 4-Nitrophenol to 4-Aminophenol. *J. Colloid Interface Sci.* **2013**, *389*, 260−267.
(6) Huang, X.; Jain, P. K.; El-Sayed, I. H.; El-Sayed, M. A. Gold Nanoparticles: Interesting Optical Properties and Recent Applications in Cancer Diagnostics and Therapy. *Nanomedicine* **2007**, *5*, 681−693.
(7) Haruta, M.; Kobayashi, T.; Sano, H.; Yamada, N. Novel Gold Catalysts for the Oxidation of Carbon Monoxide at a Temperature far Below °C. *Chem. Lett.* **1987**, *16*, 405−408.
(8) Haruta, M.; Yamada, N.; Kobayashi, T.; lijima, S. Gold Catalysts Prepared by Coprecipitation for Low-temperature Oxidation of Hydrogen and of Carbon Monoxide. *J. Catal.* **1989**, *115*, 301−309.
(9) Haruta, M. Size- and Support-Dependency in the Catalysis of Gold. *Catal. Today* **1997**, *36*, 153−166.
(10) Andreeva, D.; ldakiev, V.; Tabakova, T.; Andreev, A. Low-temperature Water-gas Shift reaction over Au/alpha Fe_2O_3. *J. Catal.* **1996**, *158*, 354−355.
(11) Ilieva-Gencheva, L.; Pantaleo, G.; Mintcheva, N.; Ivanov, I.; Venezia, A. M.; Andreeva, D. Nano-Structured Gold Catalysts Supported on CeO_2 and CeO_2-Al_2O_3 for NO_x Reduction by CO: Effect of Catalyst Pretreatment and Feed Composition. *J. Nanosci. Nanotechnol.* **2008**, *8*, 867−873.
(12) Zielasek, V.; Xu, B.; Liu, X.; Bäumer, M.; Friend, C. M. Absence of Subsurface Oxygen Effects in the Oxidation of Olefins on Au: Styrene Oxidation over Sputtered Au(111). *J. Phys. Chem. C* **2009**, *113*, 8924−8929.
(13) Kracke, P.; Haas, T.; Saltsburg, H.; Flytzani-Stephanopoulos, M. CO Oxidation on Unsupported Dendrimer-Encapsulated Gold Nanoparticles. *J. Phys. Chem. C* **2010**, *114*, 16401−16407.
(14) Korkosz, R. J.; Gilbertson, J. D.; Prasifka, K. S.; Chandler, B. D. Dendrimer Templates for Supported Au Catalysts. *Catal. Today* **2007**, *122*, 370−377.
(15) Lang, H.; Ma, R. A.; Iversen, B. L.; Chandler, B. D. Dendrimer-Encapsulated Nanoparticle Precursors to Supported Platinum Catalysts. *J. Am. Chem. Soc.* **2003**, *125*, 14832−14836.
(16) Auten, B. J.; Lang, H.; Chandler, B. D. Dendrimer Templates for Heterogeneous Catalysts: Bimetallic Pt−Au Nanoparticles on Oxide Supports. *Appl. Catal., B* **2008**, *81*, 225−235.
(17) Haruta, M. New Generation of Gold Catalysts: Nanoporous Foams and Tubes − Is Unsupported Gold Catalytically Active? *ChemPhysChem* **2007**, *8*, 1911−1913.
(18) Scott, R. W. J.; Wilson, O. M.; Crooks, R. M. Titania-supported Au and Pd Nanoparticles Synthesized from Dendrimer-Encapsulated Metal Nanoparticle Precursors. *Chem. Mater.* **2004**, *16*, 5682−5688.
(19) Dannacher, J. J. Catalytic Bleach: Most Valuable Applications for Smart Oxidation Chemistry. *J. Mol. Catal. A: Chem.* **2006**, *251*, 159−176.
(20) Blum, H.; Kramer, R. Patent Application WO 0032731, 1999.
(21) Polzer, F.; Wunder, S.; Lu, Y.; Ballauff, M. Oxidation of an Organic Dye Catalyzed by MnOx Nanoparticles. *J. Catal.* **2012**, *289*, 80−87.
(22) Segal, S. R.; Suib, S. L. Decomposition of Pinacyanol Chloride Dye Using Several Oxide Catalysts. *Chem. Mater.* **1997**, *9*, 2526−2532.
(23) Zhang, W. X.; Wang, H.; Yang, Z. H.; Wang, F. Promotion of H_2O_2 Decomposition Activity over β-MnO_2 Nanorod Catalysts. *Colloids Surf., A* **2007**, *304*, 60−66.
(24) Broughton, D. B.; Wentworth, R. L. Mechanism of Decomposition of Hydrogen Peroxide Solutions with Manganese Dioxide.I. *J. Am. Chem. Soc.* **1947**, *69*, 741−744.
(25) Do, S. H.; Batchelor, B.; Lee, H. K.; Kong, S. H. Hydrogen Peroxide Decomposition on Manganese Oxide (pyrolusite): Kinetics, Intermediates, and Mechanism. *Chemosphere* **2009**, *75*, 8−12.
(26) Zhang, W. X.; Yang, Z. H.; Wang, W.; Zhang, Y. C.; Wen, X. G.; Yang, S. H. Large-scale Synthesis of β-MnO_2 Nanorods and their Rapid and Efficient Catalytic Oxidation of Methylene Blue Dye. *Catal. Commun.* **2006**, *7*, 408−412.
(27) Janssens, T. V. W.; Clausen, B. S.; Hvolbæk, B.; Falsig, H.; Christensen, C. H.; Bligaard, T.; Nørskov, J. K. Insights into the Reactivity of Supported Au Nanoparticles: Combining Theory and Experiments. *Top. Catal.* **2007**, *44*, 15−26.
(28) Aiken, J. D.; Finke, R. G. A review of Modern Transition-Metal Nanoclusters: Their Synthesis, Characterization, and Applications in Catalysis. *J. Mol. Catal. A: Chem.* **1999**, *145*, 1−44.
(29) Manna, A.; Imae, T.; Aoi, K.; Okada, M.; Yogo, T. Synthesis of Dendrimer-Passivated Noble Metal Nanoparticles in a Polar Medium: Comparison of Size between Silver and Gold Particles. *Chem. Mater.* **2001**, *13*, 1674−1681.
(30) Kim, Y.-G.; Oh, S.-K.; Crooks, R. M. Preparation and Characterization of 1−2 nm Dendrimer-Encapsulated Gold Nanoparticles Having Very Narrow Size Distributions. *Chem. Mater.* **2004**, *16*, 167−172.
(31) Shi, X.; Wang, S.; Sun, H.; Baker, J. R. Improved Biocompatibility of Surface Functionalized Dendrimer-Entrapped Gold Nanoparticles. *Soft Matter* **2007**, *3*, 71−74.
(32) Taubert, A.; Wiesler, U.-W.; Müllen, K. Dendrimer-controlled One-pot Synthesis of Gold Nanoparticles with a Bimodal Size Distribution and Their Self-assembly in the Solid State. *J. Mater. Chem.* **2003**, *13*, 1090−1093.
(33) Crooks, R. M.; Zhao, M.; Sun, L.; Chechik, V.; Yeung, L. K. Dendrimer-Encapsulated Metal Nanoparticles: Synthesis, Characterization, and Applications to Catalysis. *Acc. Chem. Res.* **2001**, *34*, 181−190.
(34) Hervés, P.; Pérez-Lorenzo, M.; Liz-Marzán, L. M.; Dzubiella, J.; Lu, Y.; Ballauff, M. Catalysis by Metallic Nanoparticles in Aqueous Solution: Model Reactions. *Chem. Soc. Rev.* **2012**, *41*, 5577−5587.
(35) Klassen, N. V.; Marchaington, D.; H, C. E. M. H_2O_2 Determination by I_3^- Method and by $KMnO_4$ Titration. *Anal. Chem.* **1994**, *66*, 2921−2923.
(36) Rasband, W. *ImageJ, 1.47v*; National Institutes of Health: 2013.
(37) *Kinetic Studio. 2.0.8.14953*; TGK Scientific Limited: USA, 2010.
(38) *Origin Pro 8.5*; OriginLab Corperation: Northhampton, MA, 2010.
(39) Bingwa, N.; Meijboom, R. Kinetic Evaluation of Dendrimer-Encapsulated Palladium Nanoparticles in the 4-Nitrophenol Reduction Reaction. *J. Phys. Chem. C* **2014**, *118*, 19849−19858.
(40) Pande, S.; Crooks, R. M. Analysis of Poly(amidoamine) Dendrimer Structure by UV-Vis Spectroscopy. *Langmuir* **2011**, *27*, 9609−9613.
(41) Wang, Y.; Niu, S.; Zhang, Z.; Xie, Y.; Yuan, C.; Wang, H.; Fu, D. Reversible pH Manipulation of the Fluorescence Emission from Sectorial Poly(amido amine) Dendrimers. *J. Nanosci. Nanotechnol.* **2010**, *10*, 4227−4233.
(42) Esumi, K.; Suzuki, A.; Yamahira, A.; Torigoe, K. Role of Poly(amidoamine) Dendrimers for Preparing Nanoparticles of Gold, Platinum, and Silver. *Langmuir* **2000**, *16*, 2604−2608.
(43) Alvarez, M. M.; Khoury, J. T.; Schaaff, T. G.; Shafigullin, M. N.; Vezmar, I.; Whetten, R. L. Optical Absorption Spectra of Nanocrystal Gold Molecules. *J. Phys. Chem. B* **1997**, *101*, 3706−3712.
(44) Socrates, G. *Infrared and Raman Characterization Group Frequencies: Tables and Charts*, 3rd ed.; Wiley: Chichester, U.K., 2001.
(45) Leff, D. V.; Ohara, P. C.; Heath, J. R.; Gelbart, W. M. Thermodynamic Control of Gold Nanocrystal Size: Experiment and Theory. *J. Phys. Chem.* **1995**, *99*, 7036−7041.
(46) Colombini, M. P.; Andreotti, A.; Baraldi, C.; Degano, I.; Łucejko, J. J. Colour Fading in Textiles: A model Study on the Decomposition of Natural Dyes. *Microchem. J.* **2007**, *85*, 174−182.
(47) Topalovic, T. Catalytic Bleaching of Cotton: Molecular and Macroscopic Aspects. University of Twente, Ph.D Thesis, The Netherlands, 2007.
(48) Oliver-Meseguer, J.; Cabrero-Antonino, J. R.; Domínguez, I.; Leyva-Pérez, A.; Corma, A. Small Gold Clusters Formed in Solution Give Reaction Turnover Numbers of 10^7 at Room Temperature. *Science* **2012**, *338*, 1452−1455.
(49) Thathagar, M. B.; Ten-Elshof, J. E.; Rothenberg, G. Pd Nanoclusters in C-C Coupling Reactions: Proof of Leaching. *Angew. Chem., Int. Ed.* **2006**, *45*, 2886−2890.

DOI: 10.1021/acs.langmuir.5b02020
Langmuir 2015, 31, 9041−9053

(50) Feng, Z. V.; Lyon, J. L.; Crowley, J. S.; Crooks, R. M.; Bout, D. A. V.; Stevenson, K. J. Synthesis and Catalytic Evaluation of Dendrimer-Encapsulated Cu Nanoparticles. *J. Chem. Educ.* **2009**, *86*, 368−372.
(51) Rothbart, S.; Ember, E.; Van Eldik, R. Comparative Study of the Catalytic Activity of $[Mn^{II}(bpy)_2Cl_2]$ and $[Mn_2^{III/IV}(\mu\text{-}O)_2(bpy)_4](ClO_4)_3$ in the H_2O_2 Induced Oxidation of Organic Dyes in Carbonate Buffered Aqueous Solution. *Dalton Trans.* **2010**, *39*, 3264−3272.
(52) Masek, A.; Chrzescijanska, E.; Zaborski, M. Electrooxidation of Morin Hydrate at a Pt Electrode Studied by Cyclic Voltametry. *Food Chem.* **2014**, *148*, 18−23.
(53) Antonels, N. C.; Meijboom, R. Preparation of Well-Defined Dendrimer Encapsulated Ruthenium Nanoparticles and Their Evaluation in the Reduction of 4-Nitrophenol According to the Langmuir-Hinshelwood Approach. *Langmuir* **2013**, *29*, 13433−13442.
(54) Wunder, S.; Polzer, F.; Lu, Y.; Mei, Y.; Ballauff, M. Kinetic Analysis of Catalytic Reduction of 4-Nitrophenol by Metallic Nanoparticles Immobilized in Spherical Polyelectrolyte Brushes. *J. Phys. Chem. C* **2010**, *114*, 8814−8820.
(55) Laszlo, K.; Podkoscielny, P.; Dobsrowski, A. Heterogeneity of Polymer-Based Active Carbons in Adsorption of Aqueous Solutions of Phenol and 2,3,4-Trichlorophenol. *Langmuir* **2003**, *19*, 5287.
(56) Kundu, S.; Wang, K.; Liang, H. Size-Selective Synthesis and Catalytic Application of Polyelectrolyte Encapsulated Gold Nanoparticles Using Microwave Irradiation. *J. Phys. Chem. C* **2009**, *113*, 5157−5163.
(57) Liu, B. H.; Li, B. Z. A review: Hydrogen Generation from Borohydride Hydrolysis Reaction. *J. Power Sources* **2009**, *187*, 527−534.
(58) Gemeay, A. H.; El-Sharkawy, R. G.; Mansour, I. A.; Zaki, A. B. Catalytic Activity of Polyaniline/MnO_2 Composites Towards the Oxidative Decolorization of Organic Dyes. *Appl. Catal., B* **2008**, *80*, 106−115.

DOI: 10.1021/acs.langmuir.5b02020
Langmuir 2015, 31, 9041−9053